



Optical and Electrochemical Properties of Ethynylaniline Derivatives of Phenothiazine, Phenothiazine-5-oxide and Phenothiazine-5,5-dioxide

| | |
|-------------------------------|--|
| Journal: | <i>Physical Chemistry Chemical Physics</i> |
| Manuscript ID: | CP-ART-02-2014-000678.R1 |
| Article Type: | Paper |
| Date Submitted by the Author: | 07-Apr-2014 |
| Complete List of Authors: | Theriault, Kim; University of Calgary, Chemistry Sutherland, Todd; University of Calgary, Chemistry |
| | |

SCHOLARONE™
Manuscripts

Cite this: DOI: 10.1039/c0xx00000x

www.rsc.org/xxxxxx

ARTICLE TYPE

Optical and Electrochemical Properties of Ethynylaniline Derivatives of Phenothiazine, Phenothiazine-5-oxide and Phenothiazine-5,5-dioxide

Kim D. Thériault^a and Todd. C. Sutherland^{*a}

Received (in XXX, XXX) Xth XXXXXXXXX 20XX, Accepted Xth XXXXXXXXX 20XX

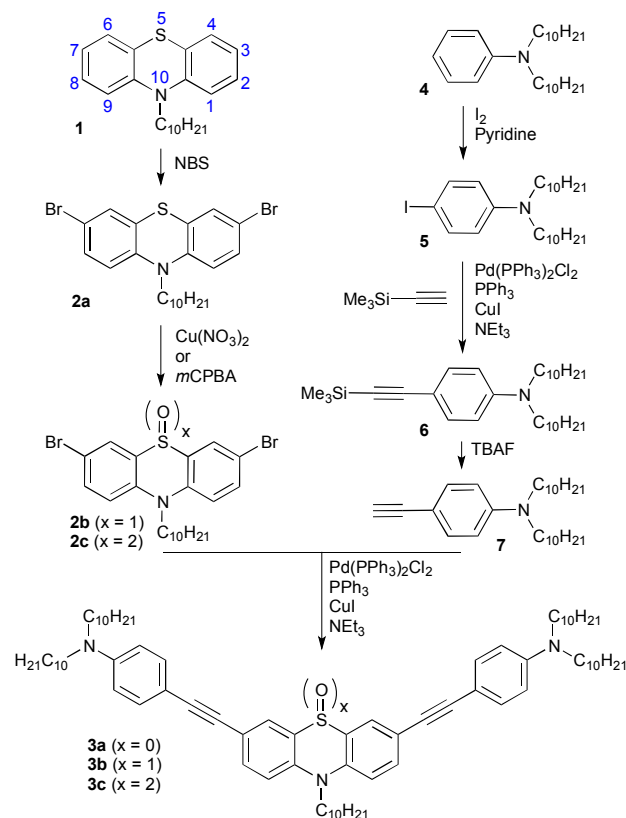
DOI: 10.1039/b000000x

Three phenothiazine (PTZ) derivatives with varying degrees of sulfur oxidation states were synthesized as strong electron donors. The thioether, sulfoxide and sulfone PTZ-derivatives exhibited irreversible oxidations at 0.19 V, 0.29 V and 0.31 V versus ferrocene, respectively. Each PTZ derivative was emissive with lifetimes of 1.7 ns, 0.5 ns, and 0.5 ns and absolute quantum yields of 0.32, 0.23 and 0.23 for the thioether, sulfoxide and the sulfone, respectively. Furthermore, these PTZ derivatives showed very large Stokes shifts ranging from 5600 cm⁻¹ to 2800 cm⁻¹. Calculations using DFT and TD-DFT methods resulted in optimized ground state and the excited state geometries of the PTZ derivatives that compared favourably to experimental optical and electrochemical data. DFT calculations revealed these butterfly shaped derivatives flatten upon excitation and this effect is greatest for the thioether PTZ derivative, resulting in the large Stokes shift. These potent electron donor systems also displayed electrochromic behaviour upon oxidation, which was attributed to a delocalized cation over the phenothiazine core and the appended ethynyl anilines. The electrochemically oxidized species had a wide absorption profile spanning from 300 nm to past 800 nm.

Introduction

Phenothiazine (PTZ) has a long and rich history, beginning in the late 19th century for its use as a dye molecule,¹ such as Lauth's violet and methylene blue. PTZ derivatives regained popularity in pharmacology due to reversal of multidrug resistance.²⁻³ More recently, PTZ was explored as an organic semiconductor because it possesses a high lying HOMO energy and was considered as an electron-donating (p-type) building block.⁴ Owing to its strong donating character, several synthetic derivatives of PTZ explored the electronic tunability by electron-donating and electron-withdrawing substituents for semiconductor applications.⁵⁻⁸

The PTZ core and its atom numbering are shown at the top of Scheme 1. Regioselective derivatization of PTZ has been extensively explored in literature and the most common substituents are at the nitrogen and the 3,7-positions. Of the over one thousand 3,7-PTZ derivatives reported, there are only ten reports of PTZ derivatized with alkyne functionality.⁹⁻¹⁸ Our approach was to install electron rich functionality, via dialkylanilines, that are bridged through a conjugated spacer to enhance the donor capability of PTZ. The alkyne spacer was deemed important to permit co-planarity between the aniline and the PTZ for more effective pi-donation. The alkyne spacer should impart desirable optical effects due to the extended conjugation and may alter the electrochemical oxidation properties. The goal of this work is to explore these PTZ derivatives as candidate electrons donors for organic electronic applications. In addition, we investigated the effect of oxidizing the sulfur in the thiazine ring to potentially access intramolecular donor-acceptor electronic interactions, as observed in phenoxazine¹⁹ and

dibenzoazaborine²⁰⁻²¹ systems.Scheme 1 Synthesis of ethynylaniline PTZ oxides **3a** – **3c**.

Structurally, the thiazine heterocycle of PTZ is non-planar and several researchers have solved single-crystal x-ray structures showing the angle between planes of the annulated benzo groups range from 138 to 156 degrees.²²⁻²⁸ The angle between planes of the annulated benzo groups of the congeners typically widens with increasing oxidation of the sulphur; 145 to 162 degrees for the sulfoxide^{29, 22, 30, 26, 31-34} and 134 – 163 degrees for the sulfone.^{23, 35-37, 32-33} However, there is significant overlap between angle ranges and the different sulfur oxidation states, implying that the thiazine ring is rather flexible and its structure is determined by both synthetic derivatization and crystal packing. Interestingly, the non-planar thiazine ring in PTZ is speculated to be responsible for the large Stokes shifts observed in the fluorescence spectra.

Here we present the synthesis of three bis-alkynylaniline PTZ derivatives, shown in Scheme 1, with the sulfur of the thiazine ring in the S(II), S(IV) and S(VI) oxidation states. The effects of the different sulfur oxidation states are explored by optical absorption spectroscopy, fluorescence spectroscopy, electrochemistry and spectroelectrochemistry and the results are interpreted by comparison to DFT-calculations. Appending dialkyl ethynylanilines to the PTZ core gives organic soluble building blocks that could lead to uniform thin films.

Results and Discussion

Synthesis

The synthesis of the ethynylaniline-PTZs, shown in Scheme 1, begins with N-alkylating PTZ under typical conditions reported by Sailer.³⁸ We elected to install decyl chains early in the synthesis to aid in organic solubility for subsequent purification steps. Regioselective electrophilic bromination also followed literature methods³⁹⁻⁴⁰ to give 3,7-dibrominated precursor **2a** in modest yields. The PTZ core building block **2a** was subjected to either mild (Cu^{2+}) or strong (*m*CPBA) oxidizing conditions, which resulted in sulfur oxidation to PTZ-5-oxide **2b**⁴¹ or PTZ-5,5-dioxide **2c**.⁴² The three different sulfur oxidation states of PTZ (**2a-2c**) were finally reacted under Sonogashira conditions with N,N-didecyl-4-ethynylaniline to give PTZ derivatives **3a** to **3c**, which are highly soluble in common organic solvents.

Optical Properties

The absorption and fluorescence spectra of **3a** to **3c** in CH_2Cl_2 are shown in figure 1 and relevant optical data are summarized in Table 1. All three PTZ derivatives show intense optical transition from 400 nm and below. Both PTZ sulfoxide and sulfone (**3b** and **3c**) show near superimposable absorption spectra, whereas compound **3a** has a different absorption profile. Clearly, the sulfur oxidation state has an effect on the intensity of the optical transitions. PTZ **3a** has the lowest energy absorption onset, calculated by the intersection between absorption and fluorescence, at 2.8 eV compared to both sulfoxide **3b** and sulfone **3c** at 3.0 eV. Each PTZ derivative is moderately fluorescent in solution with quantum yields of 0.32 for **3a** and 0.23 for both **3b** and **3c**. The fluorescence lifetime of **3a** is the longest at 1.7 ns, while **3b** and **3c** have similar lifetimes of 0.5 ns.

Most notable in the emission of **3a** is the large Stokes shift of 5600 cm^{-1} as compared to **3b** and **3c** with Stokes shifts of 2800 cm^{-1} and 2900 cm^{-1} , respectively. Such a large Stokes shift for

PTZ derivatives has been reported previously⁴³⁻⁴⁴ and is equated to a significant structural change occurring in the S_1 energy surface. The large change in structure is presumably the result of the bent ground-state structure becoming more planar in the excited state. Here, we postulate that the oxidation of the sulfur hinders the PTZ excited states from adopting the more planar structure, which results in a smaller Stokes shift for **3b** and **3c**, and these optical and structural properties are discussed further in the computational section.

Table 1: Optical properties of **3a-3c**

| Entry | $\lambda_{\text{max}} / \text{nm}$ (eV) | $\lambda_{\text{em}} / \text{nm}$ (eV) | Stokes shift / cm^{-1} | τ / ns | ϕ |
|-----------|--|---|---------------------------------------|--------------------|--------|
| 3a | 377 (3.2) /337 (3.7) | 477 (2.6) 504 (sh) | 5600 | 1.7 | 0.32 |
| 3b | 388 (3.2) / 348 (sh) | 435 (2.9) | 2800 | 0.5 | 0.23 |
| 3c | 388 (3.2) 348 (sh) | 438 (2.9) | 2900 | 0.5 | 0.23 |

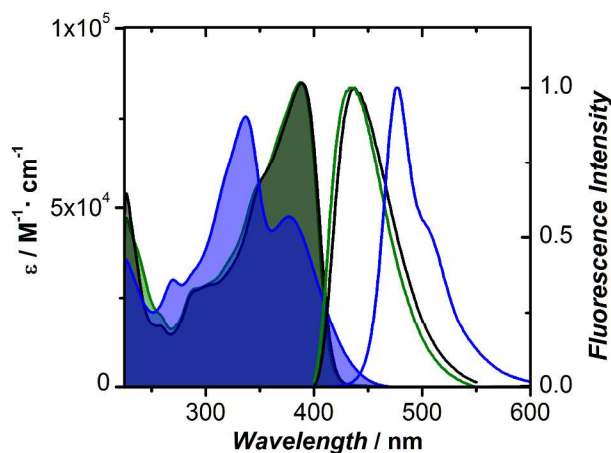


Fig. 1 Absorption and fluorescence spectra of **3a** (blue), **3b** (green) and **3c** (black) in CH_2Cl_2 . Excitation for fluorescence spectra was set at the lowest energy absorption band.

A closer examination of the fluorescence spectrum of **3a** shows a distinct peak and a lower energy shoulder, which are attributed to a vibronic side band with 1100 cm^{-1} energy spacing. The presence of vibronic bands in the fluorescence spectrum of **3a** supports the notion of a more planar or rigid structure. The absorption spectra of both **3b** and **3c** also show vibronic shoulders and peaks in the lowest energy region with an energy spacing of 2800 cm^{-1} .

Both the lowest energy absorption and emission peaks of PTZs **3a** to **3c** show solvatochromic effects, as depicted in Figure 2. The absorption energy is highest in low polarity solvents, such as hexanes, and lowest in moderate polarity CH_2Cl_2 solvent and again increases absorption energy in polar acetonitrile. The absorption bands shift by approximately 1000 cm^{-1} over the range of solvents examined. The emission profiles of **3a** to **3c** show different solvatochromic behaviour. PTZ **3a** displays small perturbations over the solvent range ($\Delta\nu_{\text{em}} = 630 \text{ cm}^{-1}$), whereas

sulfone PTZ, **3c**, exhibits a large spectral response to different solvents that span approximately 3700 cm^{-1} . PTZ **3b** has intermediary solvatochromic emission relative to **3a** and **3c**. We have elected to use the solvent dipolarity (*SdP*) empirical scale, as described by Catalán,⁴⁵ to plot the absorption and emission peaks, as shown in Figure 2. The *SdP* scale gave the most linear correlation to the absorption and emission peak data. Clearly, the single-parameter *SdP* scale does not adequately describe the complexities of the solvent interactions. Solvent effects can be divided into two interactions – specific and non-specific. Several solvent scales have been parameterized to describe the specific donor-acceptor interactions, such as Catalán's *SA*⁴⁶ and *SB*⁴⁷ scales, Kamlet and Taft's α and β ,⁴⁸⁻⁴⁹ Gutman's *AN* and *DN* scales⁵⁰ and Drago's E_B and C_B ⁵¹ scales to name a few. Non-specific interactions where solvent is treated as a dielectric continuum were originally modelled by Kirkwood⁵² and Onsager⁵³ have been empirically parameterized by Dong and Winnick's *Py* scale,⁵⁴ Kamlet, Abboud and Taft's π^* scales⁵⁵ and Drago's *S'* scale⁵⁶ and Catalán's *SPP* scale.⁵⁷ Many of the single parameter solvent scales were attempted here and resulted in poor linearity for both the absorption and emission peaks. The supporting information contains the absorption and emission spectral data for all the solvents and plots of two solvent scale approaches to demonstrate the limitations of the single-parameter solvent models in this PTZ system.

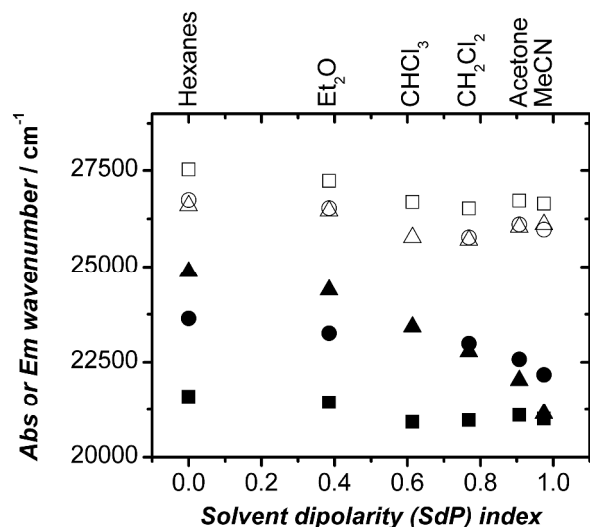


Fig. 2 Solvatochromic properties of lowest energy absorption (hollow points) and emission (solid points) bands for PTZs **3a** (squares), **3b** (circles) and **3c** (triangles) using the dipolarity index.

Instead, using Catalán's approach,⁴⁵ which combines two specific scales (*SA* and *SB*) and two general scales (*SP* and *SdP*) a multi-parameter, general approach was achieved to describe the solvent interactions for both the absorption and emission peaks. The detailed results of the fitting using the multi-parameter approach is found in the SI, but the highlights are described herein. All of the absorption peak data could be fit with non-specific scales, solvent polarizability (*SP*) and solvent dipolarizability (*SdP*), with R^2 values of 0.94 or greater. Interestingly, the emission data required the inclusion of a solvent specific scale, solvent basicity (*SB*), in addition to the non-specific *SP* and *SdP* terms to induce reasonable fits to the

emission data with R^2 values of 0.98 or greater. The *SB* term increased in significance in concert with the sulfur oxidation state in the thiazine ring, suggesting specific solvent to sulfur interactions in the excited state structure that are not present in the ground-state.

Electrochemical Properties

All three PTZ derivatives show irreversible oxidation reactions in DMF using cyclic voltammetry, as shown in the supporting information and no reduction reactions were observed within the solvent stability potential window. Oxidation potentials are reported versus an internal ferrocene/ferrocenium redox reaction using differential pulse voltammetry (DPV). PTZ derivatives **3a** to **3c** show increasing oxidation potentials of 190 mV, 285 mV and 310 mV, respectively. The stepwise increment in oxidation potential is consistent with the change in sulfur oxidation state and a stabilization of the HOMO with electron withdrawing groups. For comparison, the TMS-protected ethynyl aniline precursor shows an oxidation potential of 400 mV under the same electrochemical conditions. PTZ, under the same conditions, gives an oxidation potential of 150 mV, which is even lower than **3a** suggesting the ethynyl anilines act as electron withdrawing groups in these compounds. Since no reduction peaks were observed within the solvent stability window suggests the change in sulfur oxidation state on the thiazine ring has minimal effect on lowering the LUMO energy.

Computations

Truncated models of the three final PTZ derivatives (Me groups replaced alkyl chains) were investigated using Density Functional theory (DFT) and time-dependent (TD)-DFT calculations including solvent effects by the polarisable continuum model (PCM) at the B3LYP/6-31G+(d) level. Computational results using Gaussian09⁵⁸ with dichloromethane as the solvent provides insight into the absorption and emission energies and provide key insight into the structural changes following excitation.

All of the optimized ground state structures are butterfly-shaped about the thiazine ring, as shown in Figure 3. Note the sulfoxide derivative has two possible thiazine ring conformations: S-O bond boat-axial (**3b_{ax}**) and S-O bond boat-equatorial (**3b_{eq}**).²⁹ Calculations show a small energetic preference of 8.3 kJ mol^{-1} for the axial S-O isomer and FT-IR results, included in the ESI, were inconclusive to the isomer formed upon oxidation. The optimized ground-state structure exhibited angles between planes (calculated by the intersection of the two imaginary planes extending from the annulated benzo groups) of 145°, 141°, 149° and 148° for **3a**, **3b_{eq}**, **3b_{ax}** and **3c**, respectively, as depicted in Figure 3b. In addition, the optimized ground-state geometry resulted in dipole moments of 2.12 D, 7.69 D and 7.40 D, for **3a**, **3b_{ax}** and **3c**, respectively.

The FMOs and orbital energies are shown in Figure 3a. The thiazine derivative, **3a**, has the highest HOMO energy of the series, as expected for such an electron-rich species. There is a decrease in the HOMO energy when oxidizing to the sulfoxide and a further HOMO stabilization upon sulfone generation, leading to an overall HOMO tunability range of 0.16 eV. The limited range of HOMO energy tunability over the series of PTZs likely reflects the delocalized contributions from the ethynyl-

anilines. The HOMO coefficients of PTZs **3a** to **3c** are representative of a delocalized π -system over the entire conjugated system. Of notable difference is the coefficient on the sulfur atom in PTZ **3a**, whereas both **3b** and **3c** have nodes on sulfur. A similar decreasing energy trend in LUMO energies is found through the series of **3a** to **3c**. The LUMO shapes of **3a-3c** are nearly identical showing π -delocalized systems with nodes at

both the nitrogen and sulfur atoms of the thiazine ring. The HOMO energy levels for **3a**, **3b_{eq}**, **3b_{ax}** and **3c** using DFT 10 methods are -4.97 eV, -5.07 eV, -5.08 eV and -5.13 eV versus vacuum, respectively, compare favourably to the electrochemically-determined HOMO energy levels at -5.0 eV, -5.1 eV and -5.1 eV (using Fc/Fc⁺ redox standard at -4.8 eV)⁵⁹, for **3a** to **3c**.

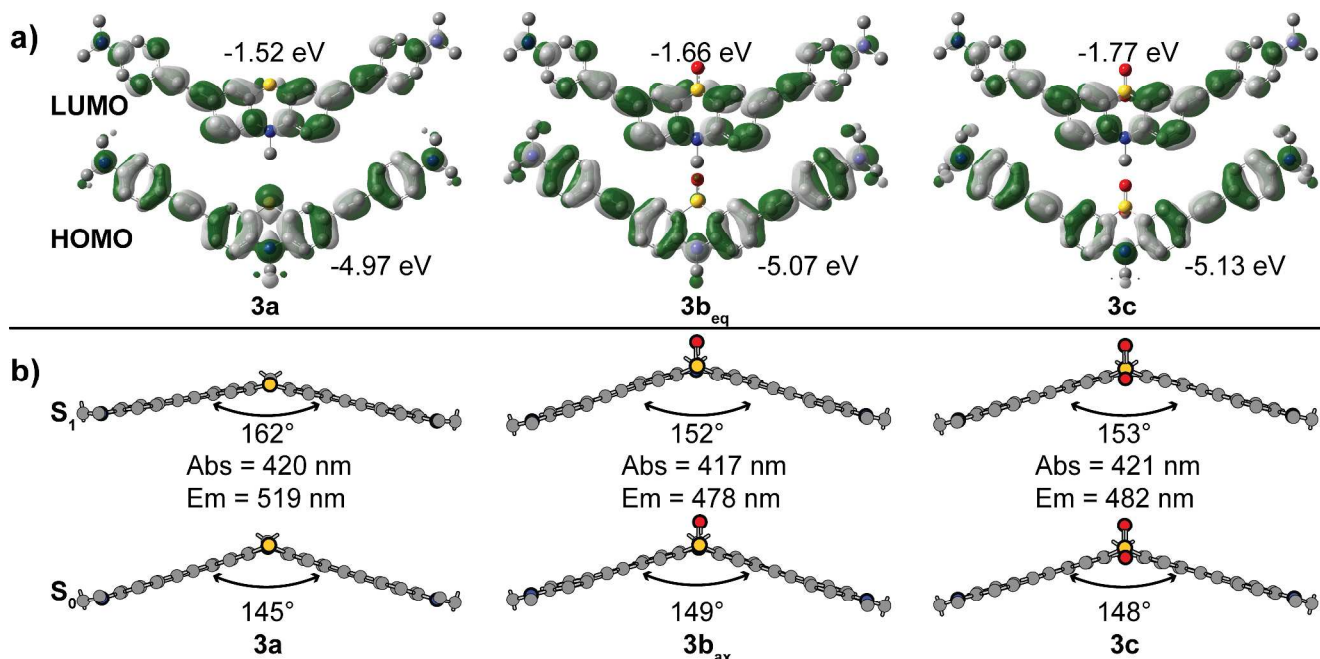


Fig. 3 a) DFT optimized ground state structures of **3a**, **3b_{eq}** and **3c**, their FMOs and orbital energies using the B3LYP/6-31G+(d,p) basis set. b) TD-DFT, using the same functional and basis set, calculations of S₀ and S₁ structures of **3a**, **3b_{ax}** and **3c** and their associated calculated absorption and emission peak energies.

TD-DFT calculations with DCM as a solvent resulted in strong 20 and exclusive HOMO to LUMO transitions in all three PTZ derivatives. The energies of the absorption transitions (S₀ to S₁) were approximately 420 nm (3.0 eV) for all of the PTZ derivatives, which is slightly lower in energy than the experimental values for **3a-3c** at 3.2 eV, determined by the λ_{max} 25 value. The first excited state structure, S₁, was then optimized in the presence of DCM and an additional TD-DFT calculation was carried out to assess the emission energy. Figure 3b summarizes the results of the TD-DFT calculations and highlights the structural changes that occur in the first excited states following 30 literature calculation methods.⁶⁰⁻⁶¹

All three PTZ derivatives exhibit significantly red-shifted emission energies compared to the absorption energies, which supports the experimentally observed Stokes shifts. Although, the absolute energy values are not directly comparable to the 35 experimental values, the same trend is apparent and the computations provide insight into the associated structural changes in the excited states. The first singlet excited state (S₁) structure of PTZ **3a** is significantly more planar compared to its ground-state, S₀, structure, which is consistent with the largest 40 Stokes shift in the series and appearance of vibronic bands in the fluorescence spectrum. The boat geometry of the thiazine ring changes from 145° to 162° in **3a**. For PTZ **3b**, both boat S-O axial and equatorial structures were computed in S₀ and S₁ states. Interestingly, only the axial structure **3b_{ax}**, mirrored both the

45 absorption and emission experimental data, supporting the notion that the Cu-mediated oxidation mechanism yields exclusively the axial product. The boat geometry of the **3b_{ax}** thiazine oxide ring changes from 149° to 152°. The S₀ and S₁ structures of the S-O boat equatorial derivative, **3b_{eq}**, as calculated by DFT methods 50 showed absorption and emission peaks at 418 nm and 497 nm, respectively. The ground state geometry of **3b_{eq}** is very similar to the **3b_{ax}** derivative; however, the S₁ optimized structure of **3b_{eq}** is more planar than the S-O axial structure leading to a significant red-shift in emission, which the experimental data does not 55 support. Clearly, the boat axial S-O of **3b_{ax}** inhibits the planarization of the PTZ leading to a small Stokes shift than **3a**. The optimized S₀ and S₁ structures of PTZ dioxide, **3c**, behaves very similarly to **3b_{ax}** with a change in boat thiazine dioxide ring geometry of 148° to 153° upon excitation. The excited-state 60 dipole moments of **3a**, **3b_{ax}** and **3c** are expectedly lower due to planarization than the S₀ structures at 0.87 D, 7.34 D and 6.79 D, respectively. Upon generation of the S₁ state, there is contraction of the thiazine of both the N-C and S-C bonds, which we speculate helps in planarization, as has been described previously 65 in the radical cation structure of PTZ.⁶²

Spectroelectrochemistry

All three final PTZ derivatives are electron donors in addition to being highly conjugated; consequently, their absorption profile changes during the oxidation reaction were investigated. The

evolutions of the absorption spectra for **3a** to **3c** are shown in figure 4. Each PTZ derivative shows the growth of an intense, red-shifted absorption profile that spans from 300 nm to over 800 nm, which is consistent with a highly delocalized cation charge. PTZ **3a** shows the most intense absorption with a broad peak centred at 680 nm. Compounds **3b** and **3c** share a similar absorption profile with peaks at 670 nm and 680 nm, respectively. Each absorption spectrum shown in figure 4 was recorded at 1 minute intervals for approximately 20 minutes. Clear isosbestic points are observed in each set of spectra at approximately 412 nm, which suggest either a stable radical cation that is electrochemically irreversible, or a chemical reaction followed the electrochemical oxidation to a new optically-active compound. Most importantly, because these alkyne anilines are able to stabilize the oxidized PTZ to such a great extent these oxidized species could find applications into potent low energy photon absorbing materials, electrochromics or as p-type molecular candidates in organic electronic applications.

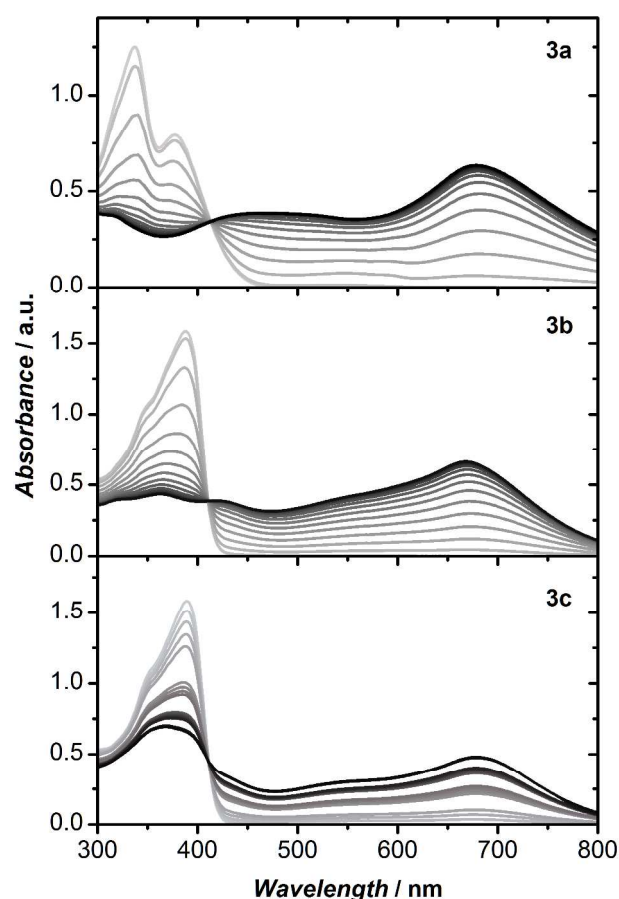


Fig. 4 Spectroelectrochemical evolution of the **3a-3c** (ca. 10^{-5} M in DMF) upon application of an oxidizing potential at the onset of oxidation determined from CV experiments. Each spectrum is taken at 1 minute intervals and the initial spectrum is a grey line that evolves to a black line over the time course of the experiment.

Conclusions

We have successfully synthesized an alkynyl aniline-PTZ

adduct by exploiting Sonogashira reaction conditions to produce a set of potent electron donating, p-type, organic semi-conductor candidates. Optically, the neutral PTZ derivatives show modest absorption properties (< 450 nm), but all derivatives are strongly emissive with large Stokes shifts up to 5600 cm^{-1} and both absorption and emission peaks are solvatochromic. All three donors exhibited irreversible oxidation potentials as low as 0.19 V vs Fc/Fc^+ and none of the PTZ derivatives displayed reductions within the solvent window, despite chemical oxidation to the thiazine-dioxide. TD-DFT calculations and optimizations show a reasonable correlation with experimental data and indicate the PTZ derivatives become more planar in the excited state, rationalizing the large Stokes shift. Furthermore, computationally-derived optical spectra support the S-O boat axial isomer over the equatorial S-O isomer. Upon electrochemical oxidation, all PTZ-derivatives exhibited a dramatic colour change owing to the delocalized cation through the PTZ core and appended ethynyl anilines that resulted in its absorption profile spanning from 300 nm to over 800 nm.

Experimental Section

Materials

All chemicals were purchased from Aldrich and used as received without further purification, aside from the following: Aniline was purchased from BHD, K_2CO_3 was purchased from EMD and $\text{Pd}(\text{PPh}_3)_2\text{Cl}_2$ was purchased from Strem. Solvents were used as received or dried using an MBraun solvent purification system. THF, DMF and DCM were stored over sieves before use and triethylamine was distilled in the presence of CaH and stored over sieves. Column chromatography was performed on SiliCycle SilicaFlash P60 silica gel (230-400 mesh). Thin-layer chromatography was carried out on Merck silica gel F_{254} aluminium-backed TLC plates.

General

NMR spectra were recorded on a Bruker 400 MHz spectrometer and referenced to residual CHCl_3 in CDCl_3 (^1H 7.26 ppm, ^{13}C 77.00) or residual $(\text{CH}_3)_2\text{CO}$ in $(\text{CD}_3)_2\text{CO}$ (^1H 2.05 ppm). Mass spectra were recorded with a Agilent 6520 LC Q-TOF spectrometer run in ESI mode by direct infusion with the column bypassed. All samples were dissolved in DCM and run with an eluent flow rate of 0.2 ml/min MeOH, source temperature 200°C , fragmenter voltage of 120 V, Nebulizer pressure of 12 psi and a drying gas flow rate of 7 L/min. FTIR spectra were recorded in diffuse reflectance mode with drop-cast films on ground KBr in a Varian FTS-7000 spectrometer. UV/Vis spectra were recorded using a Cary 5000 spectrophotometer in dual beam mode. Emission spectra were recorded using a Photon Technology International (PTI) Quanta Master spectrofluorimeter operated in CW mode, with samples in a quartz Suprasil cell (1 cm width and path length, Hellma, Canada). Lifetime measurements were obtained at room temperature using an Edinburgh Instruments FLS920 Spectrometer equipped with Fianium SC400 Super Continuum White Light Source, Hamamatsu R3809U-50 Multi Channel Plate detector and data were analyzed with Edinburgh Instruments F900 software. Curve fitting of the data was performed using a non-linear least squares procedure in the F900 software. Absolute fluorescence quantum yield values were measured using an Edinburgh Instruments FLS92 calibrated

integrating sphere S 3 system.

4: *N,N*-didecylaniline Potassium carbonate (3.0640 g, 32.9 mmol) and 1-bromodecane (25 mL, 120.8 mmol) were added to a solution of aniline (3 mL, 32.9 mmol) in DMF (100 mL) and refluxed overnight. A blue colour appeared during the reaction but disappeared after completion. The solid residues were removed by filtration followed by removal of solvent in vacuo. The crude product was then reconstituted in diethyl ether, washed with water and the organic fraction was dried with magnesium sulfate. Removal of solvent in vacuo afforded a golden oil, which was purified by silica gel column chromatography (DCM) and resulted in a light yellow oil (11.7821 g, 95.8 %).

5: *N,N*-didecyl-4-iodoaniline A solution of **4** (11.6409 g, 31.2 mmol) in dioxane:pyridine (1:1, 280 mL) was cooled in an ice bath. Iodine (19.1842 g, 75.6 mmol) was then added and the reaction mixture was stirred for 1 hour. Unreacted iodine was removed with saturated aqueous sodium thiosulfate (250 mL). Water (250 mL) was added to the organic fraction, then the product was extracted with DCM, dried with magnesium sulfate and the solvent was removed in vacuo to afford a blue oil as the crude product. Further purification with silica gel column chromatography hexanes:DCM (4:1) yielded **5** as a light yellow oil (12.1775 g, 78.2 %). ¹H NMR (400 MHz, CDCl₃) δ 7.46 (d, J = 9.1 Hz, 2H), 6.46 (d, J = 9.1 Hz, 2H), 3.30 – 3.23 (m, 4H), 1.66 – 1.55 (m, 4H), 1.43 – 1.29 (m, 28H), 0.97 (t, J = 6.9 Hz, 6H). ¹³C NMR (101 MHz, CDCl₃) δ 147.70, 137.72, 114.13, 75.53, 51.12, 32.04, 29.80, 29.78, 29.75, 29.73, 29.72, 29.70, 29.68, 29.66, 29.49, 29.48, 29.47, 29.45, 29.45, 27.29, 27.27, 27.21, 22.83, 14.26, 14.24. MS (ESI HRMS) m/z calcd for C₂₆H₄₇IN + H: 500.2748; found 500.2734.

6: *N,N*-didecyl-4-((trimethylsilyl)ethynyl)aniline A yellow mixture of **5** (9.2376 g, 18.5 mmol), bis(triphenylphosphine)palladium(II) dichloride (0.6343 g, 0.90 mmol), triphenyl phosphine (0.7295 g, 2.78 mmol) and copper (I) iodide (0.3893 g, 2.04 mmol) in dry triethylamine (50 mL) was purged with N₂. Trimethylsilylacetylene (5.3 mL, 37.2 mmol) was added by syringe over 20 minutes. The reaction mixture was stirred at room temperature and under N₂ overnight. The solvent was removed from the brown mixture in vacuo and the crude product was purified by silica gel chromatography hexanes:DCM (1:1) to give **6** as an orange oil (8.4001 g, 96.7 %). ¹H NMR (400 MHz, CDCl₃) δ 7.35 (d, J = 9.0 Hz, 2H), 6.56 (d, J = 9.0 Hz, 2H), 3.34 – 3.24 (m, 4H), 1.68 – 1.55 (m, 4H), 1.47 – 1.29 (m, 28H), 0.98 (t, J = 6.9 Hz, 6H), 0.31 (s, 9H). ¹³C NMR (101 MHz, CDCl₃) δ 148.07, 133.32, 111.10, 108.96, 107.03, 90.61, 51.00, 32.05, 29.79, 29.72, 29.65, 29.48, 27.33, 27.24, 22.82, 14.22, 0.37. MS (ESI HRMS) m/z calcd for C₃₁H₅₆NSi + H: 470.4177; found 470.4162.

7: *N,N*-didecyl-4-ethynylaniline A solution of TBAF (21 mL, 1M in THF) was added to a solution of **6** (8.4001 g, 16.8 mmol) in DCM (25 mL) and the mixture was stirred at room temperature 1 hour. The mixture was then washed with brine and H₂O, dried with magnesium sulfate and reduced in vacuo to obtain the crude product as a brown oil. The product was purified with silica gel column chromatography hexanes:DCM (1:1) to afford **7** as an orange oil (6.0262 g, 90.1 %). ¹H NMR (400 MHz, CDCl₃) δ 7.35 (d, J = 8.9 Hz, 2H), 6.55 (d, J = 9.0 Hz, 2H), 3.31 – 3.24 (m, 4H), 2.97 (s, 1H), 1.64 – 1.54 (m, 4H), 1.40 – 1.25 (m, 28H), 0.92

(t, J = 6.8 Hz, 6H). ¹³C NMR (101 MHz, CDCl₃) δ 148.34, 133.47, 111.19, 107.67, 85.21, 74.49, 51.08, 32.04, 29.80, 29.71, 29.66, 29.47, 27.34, 27.27, 22.82, 14.24. MS (ESI HRMS) m/z calcd for C₂₈H₄₈N + H: 398.3781; found 398.3770.

1: *10-decyl-10H-phenothiazine* A mixture of phenothiazine (5.1028 g, 25.6 mmol) and potassium tert-butoxide (3.1200 g, 25.6 mmol) in dry THF (50 mL) was purged with N₂ before adding 1-bromodecane (10.4 mL, 50.3 mmol). The mixture was refluxed under N₂ overnight. Removal of the solids residues by filtration and the solvent in vacuo gave a brown oil. The crude product was purified by silica gel chromatography (hexanes → hexanes:DCM (9:1)) to afford **1** as a light yellow oil (5.6460 g, 64.9 %). ¹H NMR (400 MHz, Acetone) δ 7.17 (t, J = 7.7 Hz, 2H), 7.12 (d, J = 7.6 Hz, 2H), 6.98 (d, J = 8.1 Hz, 2H), 6.92 (t, J = 7.5 Hz, 2H), 3.90 (t, J = 6.7 Hz, 2H), 1.83 – 1.71 (m, 2H), 1.50 – 1.38 (m, 2H), 1.35 – 1.18 (m, 12H), 0.87 (t, J = 6.7 Hz, 3H). ¹³C NMR (101 MHz, CDCl₃) δ 145.31, 127.37, 127.12, 124.97, 122.27, 115.37, 47.38, 31.96, 29.61, 29.55, 29.36, 29.30, 26.97, 26.91, 22.76, 14.22. MS (ESI HRMS) m/z calcd for C₂₂H₂₉NS + H: 340.2099; found 340.2071.

2a: *3,7-dibromo-10-decyl-10H-phenothiazine* A solution of **1** (3.8843 g, 11.4 mmol) in CHCl₃:AcOH (1:1, 750 mL) was cooled in an ice bath and shielded from direct light. NBS (5.4973 g, 30.9 mmol) was then added in three equal portions with an hour between each addition. One hour after the last addition of NBS, water was added when the reaction mixture was still cold. The organic layer was removed, washed with H₂O until the washes were neutral and dried with magnesium sulfate to give a red oil once the solvent was removed in vacuo. Further purification with silica gel chromatography hexanes:DCM (9:1) gave **2a** as a light yellow oil (2.7872 g, 49.0 %). ¹H NMR (400 MHz, CDCl₃) δ 7.21 (dd, J = 8.6, 2.3 Hz, 2H), 7.18 (d, J = 2.2 Hz, 2H), 6.65 (d, J = 8.6 Hz, 2H), 3.79 – 3.66 (m, 2H), 1.79 – 1.68 (m, 2H), 1.45 – 1.35 (m, 2H), 1.35 – 1.22 (m, 12H), 0.92 (t, J = 6.9 Hz, 3H). ¹³C NMR (101 MHz, CDCl₃) δ 143.79, 129.89, 129.40, 126.16, 116.39, 114.54, 47.40, 31.78, 29.41, 29.36, 29.18, 29.05, 26.66, 26.47, 22.60, 14.10. MS (ESI HRMS) m/z calcd for C₂₂H₂₇Br₂NS + H: 496.0304; found 496.0308.

2b: *3,7-dibromo-10-decyl-5-oxide-10H-phenothiazine* A solution of **2a** (1.0751 g, 2.16 mmol) and Cu(NO₃)₂·2.5 H₂O (1.4297 g, 6.15 mmol) in DCM (40 mL) was sonicated under ambient conditions for 1 hour. The solid residue was removed by filtration and the solvent was removed in vacuo to afford a yellow mixture. The crude product was purified by silica gel column chromatography DCM:EtOAc (9:1) to give **2b** as a light beige oil that solidifies upon standing (0.6849 g, 61.5 %). ¹H NMR (400 MHz, CDCl₃) δ 8.01 (d, J = 2.4 Hz, 2H), 7.68 (dd, J = 9.0, 2.4 Hz, 2H), 7.27 (d, J = 9.1 Hz, 2H), 4.16 – 4.09 (m, 2H), 1.94 – 1.83 (m, 2H), 1.53 – 1.44 (m, 2H), 1.44 – 1.22 (m, 12H), 0.89 (t, J = 6.9 Hz, 3H). ¹³C NMR (101 MHz, CDCl₃) δ 137.03, 135.82, 133.67, 125.83, 117.70, 114.01, 48.50, 31.96, 29.65, 29.59, 29.37, 29.33, 26.84, 26.33, 22.77, 14.23. MS (ESI HRMS) m/z calcd for C₂₂H₂₇Br₂NOS + H: 512.0258; found 512.0249.

2c: *3,7-dibromo-10-decyl-5,5-dioxide-10H-phenothiazine* A solution of **2a** (0.5040 g, 1.01 mmol) in DCM (10 mL) was cooled in an ice bath before addition of mCPBA (75 %, 0.7944 g, 3.45 mmol). The reaction mixture was stirred overnight as the temperature was allowed to slowly rise to room temperature. The crude product was purified by silica gel column chromatography (DCM) to give **2c** as a light brown oil (0.4317 g, 80.5 %). ¹H

NMR (400 MHz, CDCl_3) δ 8.16 (d, J = 2.4 Hz, 2H), 7.67 (dd, J = 9.1, 2.4 Hz, 2H), 7.20 (d, J = 9.1 Hz, 2H), 4.11 – 4.02 (m, 2H), 1.89 – 1.78 (m, 2H), 1.47 – 1.37 (m, 2H), 1.37 – 1.19 (m, 12H), 0.87 (t, J = 6.8 Hz, 3H). ^{13}C NMR (101 MHz, CDCl_3) δ 139.64, 136.27, 126.23, 125.51, 118.15, 114.46, 48.75, 31.94, 29.57, 29.53, 29.33, 29.22, 26.79, 26.63, 22.75, 14.22. MS (ESI HRMS) m/z calcd for $\text{C}_{22}\text{H}_{27}\text{Br}_2\text{NO}_2\text{S} + \text{Na}$: 550.0021; found 550.0020.

3a: 4,4'-(10-decyl-10H-phenothiazine-3,7-diyl)bis(ethyne-2,1-diyl)bis(*N,N*-didecylaniline) A yellow mixture of **2a** (0.5104 g, 1.03 mmol), bis(triphenylphosphine)palladium(II) dichloride (0.1539 g, 0.22 mmol), triphenyl phosphine (0.1714 g, 0.65 mmol) and copper (I) iodide (0.0713 g, 0.37 mmol) in dry triethylamine (25 mL) was purged with N_2 . A sparged solution of **7** (1.2258 g, 3.08 mmol) in triethylamine (22 mL) was added by syringe at a rate of 0.02 mL/min and left to stir for 2 weeks. Additional sparged dry triethylamine (25 mL) was added to reconstitute the solvent volume, then a second portion of a sparged solution of **7** (1.4430 g, 3.62 mmol) in dry triethylamine (22 mL) was added by syringe at a rate of 0.02 mL/min and stirred for 2 days. The solvent was removed in vacuo and the crude product was purified by silica gel chromatography hexanes:DCM (9:1 \rightarrow 3:1) to yield a viscous yellow oil (0.6493 g, 55.7 %). ^1H NMR (400 MHz, CDCl_3) δ 7.34 (d, J = 8.9 Hz, 4H), 7.30 – 7.24 (m, 2H), 7.23 (d, J = 1.9 Hz, 2H), 6.75 (d, J = 8.5 Hz, 2H), 6.57 (d, J = 9.0 Hz, 4H), 3.81 (t, J = 7.1 Hz, 2H), 3.36 – 3.20 (m, 8H), 1.86 – 1.73 (m, 2H), 1.64 – 1.53 (m, 8H), 1.48 – 1.38 (m, 2H), 1.38 – 1.21 (m, 68H), 0.95 – 0.86 (m, 15H). ^{13}C NMR (101 MHz, CDCl_3) δ 147.82, 143.95, 132.71, 130.30, 129.81, 124.09, 118.36, 114.98, 111.21, 108.86, 90.64, 86.26, 50.97, 47.62, 31.89, 29.65, 29.56, 29.51, 29.31, 29.20, 27.22, 27.14, 26.82, 22.67, 14.10. MS (ESI HRMS) m/z calcd for $\text{C}_{78}\text{H}_{119}\text{N}_3\text{S} + \text{H}$: 1130.9197; found 1130.9192.

3b: 4,4'-(10-decyl-5-oxide-10H-phenothiazine-3,7-diyl)bis(ethyne-2,1-diyl)bis(*N,N*-didecylaniline) A yellow mixture of **2b** (0.3904 g, 0.76 mmol), bis(triphenylphosphine)palladium(II) dichloride (0.0535 g, 0.076 mmol), triphenyl phosphine (0.0600 g, 0.23 mmol) and copper (I) iodide (0.0310 g, 0.16 mmol) in dry triethylamine (24 mL) was purged with N_2 . A sparged solution of **7** (0.9960 g, 2.3 mmol) in triethylamine (22 mL) was added by syringe at a rate of 0.02 mL/min while the mixture was stirred under N_2 . The solvent was removed from the brown mixture in vacuo and the crude oil was purified by silica gel chromatography DCM:EtOAc (99:1) to give **3b** as a golden oil (0.2941 g, 33.7%). **3b** is fairly stable in air but when exposed to light while in solution, it decomposes to a deep green substance. ^1H NMR (400 MHz, CDCl_3) δ 8.06 (d, J = 2.0 Hz, 2H), 7.69 (dd, J = 8.8, 2.0 Hz, 2H), 7.39 (d, J = 8.8 Hz, 4H), 7.32 (d, J = 9.0 Hz, 2H), 6.59 (d, J = 9.0 Hz, 4H), 4.22 – 4.10 (m, 2H), 3.35 – 3.22 (m, 8H), 2.00 – 1.86 (m, 2H), 1.66 – 1.55 (m, 8H), 1.55 – 1.47 (m, 2H), 1.47 – 1.39 (m, 2H), 1.39 – 1.23 (m, 66H), 0.96 – 0.87 (m, 15H). ^{13}C NMR (101 MHz, CDCl_3) δ 147.93, 136.58, 135.25, 134.35, 132.79, 124.11, 118.14, 115.60, 111.15, 108.33, 91.79, 85.55, 50.90, 31.83, 29.60, 29.51, 29.46, 29.25, 29.21, 27.16, 27.07, 26.73, 22.63, 14.06. MS (ESI HRMS) m/z calcd for $\text{C}_{78}\text{H}_{119}\text{N}_3\text{SO} + \text{H}$: 1146.9147; found 1146.9120.

3c: 4,4'-(10-decyl-5,5-dioxide-10H-phenothiazine-3,7-diyl)bis(ethyne-2,1-diyl)bis(*N,N*-didecylaniline) A yellow mixture

of **2c** (0.3039 g, 0.57 mmol), bis(triphenylphosphine)palladium(II) dichloride (0.0445 g, 0.063 mmol), triphenyl phosphine (0.0472 g, 0.18 mmol) and copper (I) iodide (0.0193 g, 0.10 mmol) in dry triethylamine (25 mL) was purged with N_2 . A sparged solution of **7** (0.7010 g, 1.76 mmol) in triethylamine (22 mL) was added by syringe at a rate of 0.02 mL/min while the mixture was stirred under N_2 . The solvent was removed from the brown mixture in vacuo and the crude product was purified by silica column chromatography hexanes:DCM (2:3) to give a yellow oil that solidifies upon standing (0.4242 g, 63.6%). ^1H NMR (400 MHz, CDCl_3) δ 8.24 (d, J = 2.0 Hz, 2H), 7.65 (dd, J = 8.9, 1.2 Hz, 2H), 7.37 (d, J = 8.9 Hz, 4H), 7.23 (d, J = 9.0 Hz, 2H), 6.58 (d, J = 9.0 Hz, 4H), 4.15 – 4.03 (m, 2H), 3.35 – 3.22 (m, 8H), 1.98 – 1.80 (m, 2H), 1.67 – 1.52 (m, 8H), 1.51 – 1.42 (m, 2H), 1.42 – 1.22 (m, 68H), 0.90 (t, J = 6.8 Hz, 15H). ^{13}C NMR (101 MHz, CDCl_3) δ 148.09, 138.90, 135.38, 132.89, 126.27, 124.19, 118.46, 115.95, 111.19, 108.14, 92.44, 85.32, 50.94, 31.87, 31.84, 29.63, 29.54, 29.49, 29.45, 29.29, 29.25, 29.15, 27.20, 27.11, 26.73, 26.60, 22.65, 14.08. MS (ESI HRMS) m/z calcd for $\text{C}_{78}\text{H}_{119}\text{N}_3\text{SO}_2 + \text{H}$: 1162.9096; found 1162.9092.

Electrochemistry

Cyclic voltammetry (CV) experiments were carried out on an Autolab PGSTAT302 potentiostat that was controlled by a PC running Autolab's GPES v 4.9 software in a temperature-controlled, three-electrode cell (15 mL). The working electrode was a Pt button, the reference electrode was a silver wire and the counter electrode was a Pt wire. All potentials were referenced to the ferrocene/ferricenium redox couple. Each CV experiment consisted of approximately 2–5 mM redox active species dissolved in 0.05 M tetrabutylammonium hexafluorophosphate in deoxygenated DMF. All CV solutions were sparged with Ar prior to dissolving the redox active species and an Ar blanket was maintained during the entire experiment. Spectroelectrochemical spectra were generated with a Cary 5000 spectrophotometer linked with a CHI 650 potentiostat using a thin layer cell (OTTLE). The working electrode, in the beam path, was a Pt mesh, a Pt wire counter electrode and a silver wire reference electrode; electrolyte and solvent as above were used.

Acknowledgements

The authors thank the NSERC Discover Grants program and KDT thanks NSERC and Alberta Innovates – Technology Futures for a postgraduate scholarship.

Notes and references

- ^a Department of Chemistry, University of Calgary, 2500 University Drive NW, Calgary Alberta, Canada. , Address, Town, Country. Fax: 01 403 289 9488; Tel: 01 403 220 7559; E-mail: todd.sutherland@ucalgary.ca
[†] Electronic Supplementary Information (ESI) available: calculated geometries of ground and excited states; cyclic voltammograms; differential pulse voltammograms; FTIR spectra; ^1H and ^{13}C NMR spectra; fluorescence Lifetime measurements. See DOI: 10.1039/b000000x/

- J. H. Stebbins, Jr., *J. Am. Chem. Soc.*, 1884, **6**, 304-305.
- J. Guan, D. E. Kyle, L. Gerena, Q. Zhang, W. K. Milhous and A. J. Lin, *J. Med. Chem.*, 2002, **45**, 2741-2748.

- 3 M. Viveiros and L. Amaral, *Int. J. Antimicrob. Agents*, 2001, **17**, 225-228.
- 4 M. Lee, J. E. Park, C. Park and H. C. Choi, *Langmuir*, 2013, **29**, 9967-9971.
- 5 A. S. Hart, C. C. B. K, N. K. Subbaiyan, P. A. Karr and F. D'Souza, *ACS Appl. Mater. Interfaces*, 2012, **4**, 5813-5820.
- 6 A. Tacca, R. Po, M. Caldararo, S. Chiaberge, L. Gila, L. Longo, P. R. Mussini, A. Pellegrino, N. Perin, M. Salvalaggio, A. Savoini and S. Spera, *Electrochim. Acta*, 2011, **56**, 6638-6653.
- 7 Z. Wan, C. Jia, Y. Duan, J. Zhang, Y. Lin and Y. Shi, *Dyes Pigm.*, 2012, **94**, 150-155.
- 8 F. Xu, C. Wang, L. Yang, S. Yin, A. Wedel, S. Janietz, H. Krueger and Y. Hua, *Synth. Met.*, 2005, **152**, 221-224.
- 9 C. S. Barkschat, S. Stoycheva, M. Himmelhaus and T. J. J. Mueller, *Chem. Mater.*, 2010, **22**, 52-63.
- 10 N. Bucci and T. J. J. Mueller, *Tetrahedron Lett.*, 2006, **47**, 8329-8332.
- 11 C. S. Kraemer and T. J. J. Mueller, *Eur. J. Org. Chem.*, 2003, 3534-3548.
- 12 C. S. Kraemer, K. Zeitler and T. J. J. Mueller, *Org. Lett.*, 2000, **2**, 3723-3726.
- 13 X. Ma, X. Mao, S. Zhang, X. Huang, Y. Cheng and C. Zhu, *Polym. Chem.*, 2013, **4**, 520-527.
- 14 T. J. J. Muller, *Tetrahedron Lett.*, 1999, **40**, 6563-6566.
- 15 M. Song, J. S. Park, Y. H. Kim, M. A. Karim, S.-H. Jin, R. S. Ree, Y. R. Cho, Y.-S. Gal and J. W. Lee, *Macromol. Res.*, 2011, **19**, 654-659.
- 16 W.-Y. Wong, W.-C. Chow, K.-Y. Cheung, M.-K. Fung, A. B. Djuricic and W.-K. Chan, *J. Organomet. Chem.*, 2009, **694**, 2717-2726.
- 17 W.-W. Zhang, W.-L. Mao, Y.-X. Hu, Z.-Q. Tian, Z.-L. Wang and Q.-J. Meng, *J. Phys. Chem. A*, 2009, **113**, 9997-10004.
- 18 W.-W. Zhang, Y.-G. Yu, Z.-D. Lu, W.-L. Mao, Y.-Z. Li and Q.-J. Meng, *Organometallics*, 2007, **26**, 865-873.
- 19 Y. Zhu, A. P. Kulkarni, P.-T. Wu and S. A. Jenekhe, *Chem. Mater.*, 2008, **20**, 4200-4211.
- 20 T. Agou, J. Kobayashi and T. Kawashima, *Chem. Commun. (Cambridge, U. K.)*, 2007, 3204-3206.
- 21 T. Agou, T. Kojima, J. Kobayashi and T. Kawashima, *Org. Lett.*, 2009, **11**, 3534-3537.
- 22 S. G. Dahl, E. Hough and P.-A. Hals, *Biochem. Pharmacol.*, 1986, **35**, 1263-1269.
- 23 K. T. Kamtekar, K. Dahms, A. S. Batsanov, V. Jankus, H. L. Vaughan, A. P. Monkman and M. R. Bryce, *J. Polym. Sci., Part A: Polym. Chem.*, 2011, **49**, 1129-1137.
- 24 Christa S. Krämer and Thomas J. J. Müller, *Eur. J. Org. Chem.*, 2003, **2003**, 3534-3548.
- 25 C. S. Krämer, K. Zeitler and T. J. J. Müller, *Org. Lett.*, 2000, **2**, 3723-3726.
- 26 T. Okuno, S. Ikeda, N. Kubo and D. J. Sandman, *Molecular Crystals and Liquid Crystals*, 2006, **456**, 35-44.
- 27 S. Umezono and T. Okuno, *Acta Crystallographica Section E*, 2012, **68**, o2790.
- 28 W.-W. Zhang, Y.-G. Yu, Z.-D. Lu, W.-L. Mao, Y.-Z. Li and Q.-J. Meng, *Organometallics*, 2007, **26**, 865-873.
- 29 S. S. C. Chu, P. De Meester, M. V. Jovanovic and E. R. Biehl, *Acta Crystallographica Section C*, 1985, **41**, 1111-1114.
- 30 E. Hough, M. Hjorth and S. G. Dahl, *Acta Crystallographica Section B*, 1982, **38**, 2424-2428.
- 31 H. Tabata and T. Okuno, *Acta Crystallographica Section E*, 2012, **68**, o2214.
- 32 S. Umezono, S. Ikeda and T. Okuno, *Acta Crystallographica Section C*, 2013, **69**, 1553-1556.
- 33 S. Umezono and T. Okuno, *J. Mol. Struct.*, 2013, **1049**, 293-298.
- 34 Z. Xu, Y. Sun, L. Yang and Q. Wang, *Acta Crystallographica Section E*, 2009, **65**, o1799.
- 35 M. S. Siddegowda, R. J. Butcher, M. Akkurt, H. S. Yathirajan and A. R. Ramesh, *Acta Crystallographica Section E*, 2011, **67**, o1875.
- 36 M. S. Siddegowda, J. P. Jasinski, J. A. Golen and H. S. Yathirajan, *Acta Crystallographica Section E*, 2011, **67**, o1702.
- 37 H. Tabata and T. Okuno, *Acta Crystallographica Section E*, 2012, **68**, o2519.
- 38 M. Sailer, A. W. Franz and T. J. J. Müller, *Chemistry – A European Journal*, 2008, **14**, 2602-2614.
- 39 S. A. Elkassih, P. Sista, H. D. Magurudeniya, A. Papadimitratos, A. A. Zakhidov, M. C. Biewer and M. C. Stefan, *Macromol. Chem. Phys.*, 2013, **214**, 572-577.
- 40 S.-K. Son, Y.-S. Choi, W.-H. Lee, Y. Hong, J.-R. Kim, W.-S. Shin, S.-J. Moon, D.-H. Hwang and I.-N. Kang, *J. Polym. Sci., Part A: Polym. Chem.*, 2010, **48**, 635-646.
- 41 L. Gaina, A. Csampai, G. Turos, T. Lovasz, V. Zsoldos-Mady, I. A. Silberg and P. Sohar, *Organic & Biomolecular Chemistry*, 2006, **4**, 4375-4386.
- 42 T. Ishihara, H. Kakuta, H. Moritani, T. Ugawa and I. Yanagisawa, *Chem. Pharm. Bull.*, 2004, **52**, 1204-1209.
- 43 M. Hauck, M. Stolte, J. Schönhaber, H.-G. Kuball and T. J. J. Müller, *Chemistry – A European Journal*, 2011, **17**, 9984-9998.
- 44 L. Yang, J.-K. Feng and A.-M. Ren, *The Journal of Organic Chemistry*, 2005, **70**, 5987-5996.
- 45 J. Catalán, *The Journal of Physical Chemistry B*, 2009, **113**, 5951-5960.
- 46 J. Catalán and C. Díaz, *Liebigs Annalen*, 1997, **1997**, 1941-1949.
- 47 J. Catalán, C. Díaz, V. López, P. Pérez, J.-L. G. De Paz and J. G. Rodríguez, *Liebigs Annalen*, 1996, **1996**, 1785-1794.
- 48 M. J. Kamlet and R. W. Taft, *J. Am. Chem. Soc.*, 1976, **98**, 377-383.
- 49 R. W. Taft and M. J. Kamlet, *J. Am. Chem. Soc.*, 1976, **98**, 2886-2894.
- 50 V. Gutmann, *Coord. Chem. Rev.*, 1976, **18**, 225-255.
- 51 R. S. Drago, *Applications of Electrostatic-covalent Models in Chemistry*, Surfside Scientific Publishers, 1994.
- 52 J. G. Kirkwood, *The Journal of Chemical Physics*, 1934, **2**, 351-361.
- 53 L. Onsager, *J. Am. Chem. Soc.*, 1936, **58**, 1486-1493.
- 54 D. C. Dong and M. A. Winnik, *Can. J. Chem.*, 1984, **62**, 2560-2565.
- 55 M. J. Kamlet, J. L. Abboud and R. W. Taft, *J. Am. Chem. Soc.*, 1977, **99**, 6027-6038.
- 56 R. S. Drago, *Journal of the Chemical Society, Perkin Transactions 2*, 1992, 1827-1838.
- 57 J. Catalán, V. López, P. Pérez, R. Martín-Villamil and J.-G. Rodríguez, *Liebigs Annalen*, 1995, **1995**, 241-252.
- 58 M. J. Frisch, G. W. Trucks, H. B. Schlegel, G. E. Scuseria, M. A. Robb, J. R. Cheeseman, G. Scalmani, V. Barone, B. Mennucci, G. A. Petersson, H. Nakatsuji, M. Caricato, X. Li, H. P. Hratchian, A. F. Izmaylov, J. Bloino, G. Zheng, J. L. Sonnenberg, M. Hada, M. Ehara, K.

- Toyota, R. Fukuda, J. Hasegawa, M. Ishida, T. Nakajima, Y. Honda, O. Kitao, H. Nakai, T. Vreven, J. A. Montgomery, J. E. Peralta, F. Ogliaro, M. Bearpark, J. J. Heyd, E. Brothers, K. N. Kudin, V. N. Staroverov, R. Kobayashi, J. Normand, K. Raghavachari, A. Rendell, J. C. Burant, S. S. Iyengar, J. Tomasi, M. Cossi, N. Rega, J. M. Millam, M. Klene, J. E. Knox, J. B. Cross, V. Bakken, C. Adamo, J. Jaramillo, R. Gomperts, R. E. Stratmann, O. Yazyev, A. J. Austin, R. Cammi, C. Pomelli, J. W. Ochterski, R. L. Martin, K. Morokuma, V. G. Zakrzewski, G. A. Voth, P. Salvador, J. J. Dannenberg, S. Dapprich, A. D. Daniels, Farkas, J. B.
- 10 Foresman, J. V. Ortiz, J. Cioslowski and D. J. Fox, Gaussian, Inc., Wallingford CT, 2009.
- 59 S. Trasatti, *Pure & Appl. Chem.*, 1986, **58**, 955-966.
- 60 T. Le Bahers, T. Pauporte, G. Scalmani, C. Adamo and I. Ciofini, *PCCP*, 2009, **11**, 11276-11284.
- 15 61 A. Pedone, J. Bloino, S. Monti, G. Prampolini and V. Barone, *PCCP*, 2010, **12**, 1000-1006.
- 62 D. Pan and D. L. Phillips, *The Journal of Physical Chemistry A*, 1999, **103**, 4737-4743.

20